ASME Journal of Mechanisms and Robotics
Online journal at:
https://asmedigitalcollection.asme.org/mechanismsrobotics

Sekar Anup Chander
Manufacturing Science and Instrumentation Division,
CSIR-Central Scientific Instruments Organisation,
Sector-30C, Chandigarh 160030, India;
Academy of Scientific and Innovative Research (AcSIR),
Ghaziabad, Uttar Pradesh 201002, India
e-mail: anup@csio.res.in

Ashutosh Mukherjee
RWTH Aachen University,
Aachen,
North Rhine-Westphalia 52056, Germany
e-mail: ashutosh.mukherjee@rwth-aachen.de

Vhatkar Dattatraya Shivling
Intelligent Machines and Communication Systems Division,
CSIR-Central Scientific Instruments Organisation,
Sector-30C, Chandigarh 160030, India;
Academy of Scientific and Innovative Research (AcSIR),
Ghaziabad, Uttar Pradesh 201002, India
e-mail: vvdatta@csio.res.in

Ashish Singla[1]
Department of Mechanical Engineering,
Thapar Institute of Engineering and Technology,
Patiala, Punjab 147004, India
e-mail: ashish.singla@thapar.edu

Enhanced Euler–Lagrange Formulation for Analyzing Human Gait With Moving Base Reference

Euler–Lagrange's formulation is known for its systematic and simplified approach to deriving dynamics of complex systems. In order to apply the existing formulation to human gait dynamics, the base reference frame must be assumed as an inertial reference frame. Conventionally, the ankle joints or the hip joints are regarded as base reference frames during the stance and swing phases of human walking. As these joints are non-inertial in nature during actual locomotion, this assumption could result in inaccurate calculation of lower-limb joint torques and forces. Therefore, in this paper, an existing Euler–Lagrange-based formulation originally developed for fixed-base robotic manipulators is considered and modified to accommodate the movement of the base reference frame with respect to an inertial frame of reference defined outside the human body. The applicability of the modified formulation is studied, implemented, and validated using three standard and publicly available gait datasets covering the phases of walking and running. The joint torques obtained using the proposed dynamic model are compared with reference torques by calculating the mean absolute error values and visually through Bland–Altman plots. The obtained joint torque values and plots indicate a close agreement with published torques, thereby validating the accuracy of the proposed dynamic model. The robust formulation implementation makes it a valuable resource for researchers in this field, offering a reliable framework for gait analysis and the design of lower-limb prosthetics or exoskeletons. [DOI: 10.1115/1.4065520]

Keywords: Euler–Lagrange formulation, human gait, inverse dynamic model, Marker data, moving frame reference, kinematics, dynamics, and control of mechanical systems, multi-body dynamics and exoskeletons, rehabilitation mechanisms and robots, theoretical and computational kinematics

Introduction

The study of human gait provides greater insights into the health, balance, and functional ability of an individual. Though studies show that human walking is the simplest form of gait [1], the complete locomotion process involves detailed coordination and control among multiple body segments, muscles, and neural control systems. The gait is assessed both through visual observation and the combination of motion capture systems along with force plates. An important parameter used for the assessment of human dynamics is the estimation of joint torques during the gait. They provide valuable quantified information required for assessing patients. The joint torque values are of great use in rehabilitation, and also toward design of lower-limb prosthetics or exoskeleton. Consequently, this necessitates the development of inverse dynamics models of human gait.

Human gait models and humanoid robots (HR) share similarities in segmented body structure, joint dynamics, stability, and control strategies. Models developed for one are often used for the other. Deep learning models like reinforcement learning (RL) have been used to balance the lower body of the HR with 12 degrees-of-freedom [2], using symbolic inverse kinematics and the RL model instead of direct joint torque estimation. Similarly, in the case of human walking long-short term memory neural-network models were trained to estimate joint torques from Electromyography (EMG) and joint angles during walking [3]. In this paper, the authors emphasize an analytical method for calculating joint torques based on kinematic motion data and estimated body-segment parameters of the human body. The proposed analytical model could serve as a benchmark for neural network models and can enrich them by integrating physical insights into neural network training.

One of the common analytical methods of modeling human walking or a biped is the inverted pendulum (IP) method [4]. IP models assume the entire body rotates about the ankle joint and that the motion occurs primarily in the sagittal plane, thereby modeling by simplifying the complexity of actual human walking. Spring-loaded inverted pendulum models were developed to overcome the limitation of a simple inverted pendulum model, where

[1]Corresponding author.

Contributed by the Mechanisms and Robotics Committee of ASME for publication in the Journal of Mechanisms and Robotics. Manuscript received January 22, 2024; final manuscript received May 13, 2024; published online June 19, 2024. Assoc. Editor: C. P. Vyasarayani.

the distance between the hip and pivot is not constant [5]. A nonlinear inverted pendulum model for uneven deformable terrain was presented by Gora et al. [6]. The IP models primarily addressed the stability and energetics of human gait or biped. In order to understand the specific roles of individual joints and muscles in human motion, multi-segment models were developed.

In one of the multi-segment models of human gait, the body was represented as a combination of 13 rigid segments comprising the head, torso, pelvis, upper arms, forearms, thighs, shank, and feet [7]. The dynamics of each segment were determined using force-balance equations. Similarly, joint torques derived using 2D and 3D models were studied using the free-body-segment method to understand the difference in torque values of both models [8]. Considering the motion of the lower limb alone, the swing phase of the leg was modeled as a compound pendulum in the work by Maillardet [9]. In the same work, the motion of the legs is considered in the sagittal plane, and the hip is assumed to move with uniform velocity in the direction of locomotion. The joint reaction forces and muscle moments were calculated using this assumption. In addition to treating the lower limb as individual segments, viscoelastic parameters were incorporated for the hip, knee, and ankle joints to explore their correlation with the gait pattern [10]. Though the multi-segment models were employed to compute the joint torques, they were tailored to each type of segment model. Describing the human body as a mechanical multi-body system enables us to establish its equations of motion using conventional formulations of used for modeling robotic manipulators, such as the Newton–Euler (N–E) or the Euler–Lagrange (E–L) formulation methods.

Both N–E and E–L methods use Denavit–Hartenberg (D–H) parameters to formulate the kinematic model of human gait. N–E formulation for dynamics involves both forward and backward recursive equations, with intricate vector cross-product terms. The equations of motion of each segment are derived in steps using the d'Alembert principle and set of equations, describing the relation between moving segments with respect to base coordinate frame. Alternatively, E–L formulation is an energy-based approach, known for its simple and systematic nature [11]. With this formulation, the system dynamics are simplified into a single procedure, independent of the number of segments considered or the type of coordinates used [12].

In previous studies using E–L formulation for human gait, Al-Shuka et al. [13] utilized the formulation to derive the equations of motion for biped robots. The foot was assumed to be in full contact with the ground, and therefore considered as inertial reference frame during single support phase. The human motion was considered to behave like a closed-chain mechanism during the double support phase. Xiang et al. [14] used E–L formulation to analyze a spatial digital human model with various kinematical and physical constraints. They utilized the same formulation to compute ground reaction forces (GRF), ensuring the overall equilibrium of the human model. Furthermore, apart from its application in human gait modeling, the E–L formulation was utilized to derive dynamic equations for the coupled human-exoskeleton system [15]. Velandia et al. [16] presented their research where Euler–Lagrange equations were used to model the exoskeleton. Their work also highlighted that E–L equations enable the convenient design of robust controllers.

A commonly used E–L formulation for robotic manipulators is presented in the work by Fu et al. [11]. The motion equations from this formulation yield explicit state equations for gait dynamics, enabling the design of advanced control strategies in the joint-variable space. Tutsoy and Barkana [17] presented their research where an under-actuated manipulator was modeled using E–L technique and represented the system in state-space for control purposes, addressing the stability and chaotic regions of the manipulator. E–L formulation is usually expressed in the form of matrix mathematics, thereby allowing direct computational implementation. In the previous papers where E–L formulation was used, the researchers assumed the base frame to be an inertial reference frame, with respect to which the dynamic equations are derived. In gait dynamic studies using E–L formulations, it can be observed that the foot is considered as the reference base frame during the stance phase. Conversely, during the swing phase, the hip is assumed to be the base frame of reference for deriving the dynamic equations. Since the base frame on the hip is not inertial in nature during actual human gait, the movement of hip frame with respect to an inertial frame needs to be compensated in the derivation of joint torques using E–L formulation.

The concept of moving base frame has been discussed in the case of humanoids or satellites. In this case, a new 6DOF joint is used in between the fixed and floating base [18]. Recursive N–E algorithm formulation was used to derive the dynamic equations. In the case of floating-base humanoids, where the base is not fixed to the ground, the robot's control was treated like an optimization problem [19]. Lagrange multipliers are used for finding local minima and maxima of a function subject to constraints, whereas the E–L formulation is used to derive the equations of motion of a system. However, Lagrange multipliers are used for computing GRF during human gait [20]. It can be noticed that E–L formulations have been utilized for fixed frame systems in the context of robotic manipulators, while they are applied with the assumption of the moving base frame being inertial in the case of human motion. However, a comprehensive Euler–Lagrange formulation for a moving base human motion has not been addressed in the existing literature.

Therefore, in order to utilize the advantages of E–L formulation in developing the dynamic model of human walking, in this work, the hip joint is considered as the reference base frame, and its motion with respect to some other inertial frame outside the body is included in the dynamic model so as to accommodate its motion parameters. During the development of the model for human walking, insights from the dynamic model of robotic manipulators with a moving base by Wronka and Dunnigan [21] were incorporated. In order to validate the proposed model for different phases of human gait, three different standard and published datasets were used. The datasets comprised marker data of lower-limb joints, GRF data, and center-of-pressure (COP) marker data, recorded at different time stamps or percentage values of the gait cycle. The major contributions of the current work are as follows:

- **Modification of existing manipulator dynamic model to accommodate for moving base frame:** The E–L formulation-based manipulator dynamics model is adapted such that the base reference frame on the hip joint is transformed into a non-inertial frame, so that the model can be applied for human gait analysis.
- **Validation using experimental and simulated datasets:** The new modified framework is substantiated through validation using three standard gait datasets, pertaining to both walking and running. The joint torques obtained are compared with reference torques by means of Bland–Altman plots and by calculating the mean absolute error (MAE). Therefore, the results are analyzed both visually and quantitatively.

The paper is structured as follows. In "Mathematical Modeling of Human Gait" section, the mathematical modeling of gait along with the kinematic and dynamic aspects is detailed. "Results and Discussion" section describes the validation of the proposed model using three datasets of human gait available in the literature. The results after simulation using the proposed model are presented using comparison plots and Bland–Altman plots. "Conclusion" section concludes the findings from this research work.

Mathematical Modeling of Human Gait

Planar Model of Human Gait. In this paper, human motion is considered in the sagittal plane, where the lower limb is represented as a rigid three-link serial manipulator with the thigh, shank, and foot as the rigid links as shown in Fig. 1(*a*). They are assumed to be connected by means of three rotational joints—hip, knee, and ankle joints when analysis of a single leg is considered. As only

the sagittal plane motions are analyzed, the system has three independent rotational degrees-of-freedom. In order to establish the relation between adjacent links or segments, the coordinate frames are affixed to the joints connecting the links or segments. The coordinate frames are established such that

(a) z_{i-1}-axis is along the axis of motion of ith joint;
(b) x_i-axis such that it is normal to z_{i-1}-axis;
(c) y_i-axis is such that the right-hand coordinate system is completed.

In this paper, the z_0-axis is considered to lie along the axis of rotational motion of the hip joint. The motion of all other segments of the leg is considered with respect to the hip joint coordinates, which is assumed to be the base frame for the system. The procedure followed for assigning the link coordinate system is as per the D–H representation outlined in the book by Fu et al. [11]. After assigning the coordinate system, the D–H parameters are used to formulate the forward kinematics of the system (Table 1). The D–H transformation arm matrix **A** relating the ith frame and $(i-1)$th frame is given by

$$ {}^{i-1}\mathbf{A}_i = \begin{bmatrix} \cos\theta_i & -\cos\alpha_i \sin\theta_i & \sin\alpha_i \sin\theta_i & a_i \cos\theta_i \\ \sin\theta_i & \cos\alpha_i \cos\theta_i & -\sin\alpha_i \cos\theta_i & a_i \sin\theta_i \\ 0 & \sin\alpha_i & \cos\alpha_i & d_i \\ 0 & 0 & 0 & 1 \end{bmatrix} \tag{1} $$

where

θ_i = joint parameter from the x_{i-1} -axis to the x_i -axis about z_{i-1}
d_i = distance from x_{i-1} to x_i measured along z_{i-1}
α_i = angle from z_{i-1} -axis to the z_i -axis about x_i
a_i = distance from z_{i-1} -axis to the z_i-axis about x_i

Table 1 D–H parameter table of the leg model in the sagittal plane

Joint i	θ_i	α_i	d_i	a_i
1	θ_1	0	L_1	0
2	θ_2	0	L_2	0
3	θ_3	0	L_3	0

As the joints of the human leg are assumed to be a sequence of single-axis rotation joints [22], θ_i is the joint parameter that changes as link i moves with respect to link $(i-1)$. These joint parameters are linearly dependent on the joint angles for the lower limb. The joint angles can be calculated using the law of cosines from the marker data [23]. Another technique to calculate the joint angles is using the absolute angle of a specific limb segment [12]. In this paper, the segment angles are calculated first, which are then used to calculate the joint angles. The angle of the segment in space with respect to horizontal axes is given by

$$ \theta_{segment} = \tan^{-1}\left(\frac{y_i - y_j}{x_i - x_j}\right) \tag{2} $$

where $(x_i,\ y_i)$, $(x_j,\ y_j)$ are the end-point coordinates of the segment under consideration. From the segment angles which are absolute in the spatial reference system, the joint angles are calculated between two adjacent segments. The hip, knee, and ankle joint angles respectively can be calculated using the following equations:

$$ \theta_{hip} = \theta_{21} \tag{3} $$

$$ \theta_{knee} = \theta_{21} - \theta_{32} \tag{4} $$

$$ \theta_{ankle} = \theta_{32} - \theta_{54} + 90 \text{ deg} \tag{5} $$

where θ_{21} is the thigh segment angle, θ_{32} is the shank segment angle, and θ_{54} is the slope of the line joining marker-4 and marker-5 as shown in Fig. 1(*a*). Another input that goes into defining the link parameters is the link length, which is calculated using the algebraic distance formula between two points (markers). With the data of joint coordinates and joint angles, their time derivatives are calculated if the velocity or acceleration values are not provided. A commonly used numerical technique to compute the time derivatives is the central-difference method.

Dynamics of the Human Lower-Limb Model. The Euler–Lagrange-based dynamic formulation used in this study to obtain the dynamics of the lower limb is inspired by the work of Fu et al. [11]. For the dynamic formulation introduced ahead, the hip joint frame is always considered as the reference base frame. After obtaining the transformation matrices using the joint angles and segment lengths, the joint moments are calculated. The

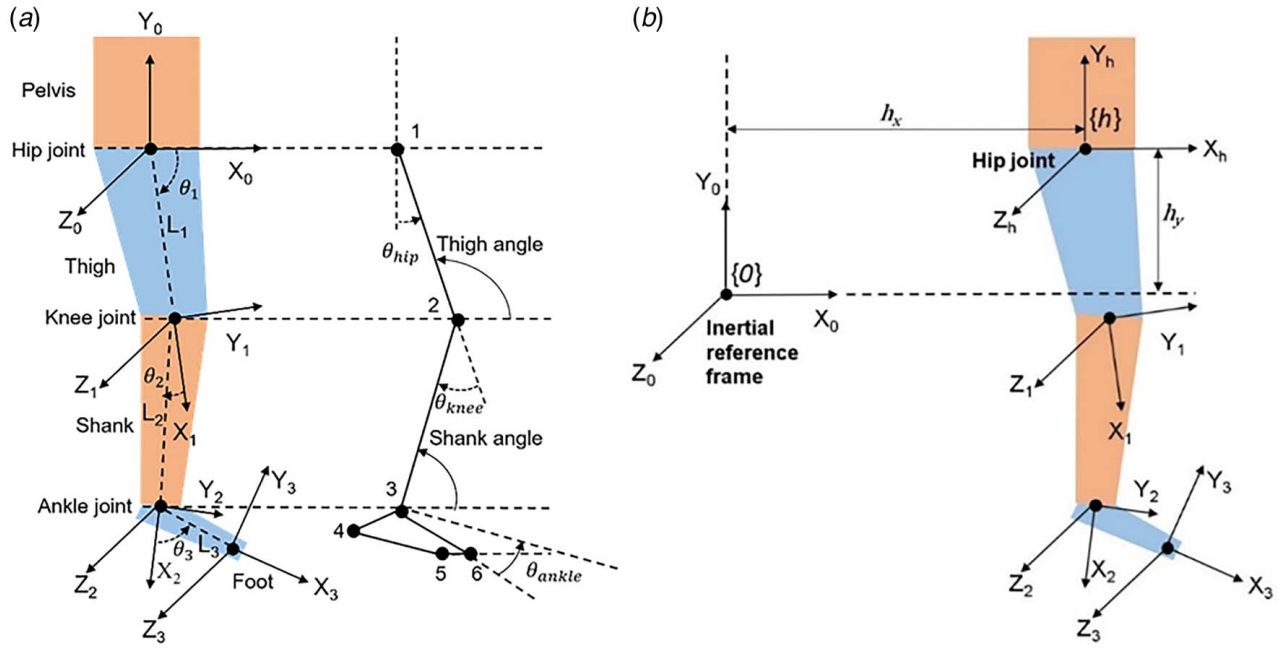

Fig. 1 (*a*) Four-link model of the leg and (*b*) movement of the lower limb with respect to inertial reference frame

additional parameters that go as input in the formulation of dynamic equations are the segment masses, center-of-mass location of each segment, and respective moments of inertia. The segment masses are estimated as a percentage of the total body mass [24,25]. The location of the center of mass (COM) from the proximal joint is also estimated as a percentage of segment length [26]. These segment parameters are now used as input in the formulation of dynamic equations for calculating the joint torques.

Furthermore, the dynamic formulation introduced ahead makes some assumptions in order to simplify the problem. These are:

(a) The gait, which actually is a three-dimensional motion is assumed to be a two-dimensional motion happening only in the sagittal plane.
(b) All segments are assumed to resemble cylindrical rods with negligible diameter, i.e., the moment of inertia of each segment about its axis is negligible, while the other two principal moments of inertia are equal to each other.
(c) The friction and other dissipative elements present within each joint are assumed to be negligible.
(d) The inertia of the upper body is assumed to be much higher than the inertia of the lower limbs, i.e., the motion of the lower limbs is assumed to not affect the motion of the upper torso at all.
(e) The hip is always considered to be the (non-inertial) reference base frame with respect to which the kinematics and the dynamics of the lower limb are computed and whose orientation at all times remains the same with respect to the inertial frame of reference. The illustration of the frames is shown in Fig. 1(*b*).
(f) The trajectory of the hip joint and its derivatives are not considered as part of the generalized coordinate vector, instead, they are considered to be model parameters.

In the equations presented, scalars are denoted in small-caps and italicized font, vectors in small-caps, bold, and italicized font, and matrices in capital and bold font. As E–L formulation is used to derive the gait dynamics, the equation to derive the joint torques is given by Eq. (6)

$$\tau_i = \frac{d}{dt}\left(\frac{\partial L}{\partial \dot{q}_i}\right) - \frac{\partial L}{\partial q_i}, \quad \forall\, i = 1,\ 2,\ \ldots,\ n \tag{6}$$

where the Lagrangian function "L" is the difference between total kinetic energy (K) and total potential energy (P) of the system under consideration. The generalized coordinate "q_i" in this study is the joint angle "θ_i". To compute the kinetic energy of the lower limb, it is required to compute the joint velocity "v_i" of each segment. If ${}^{O}\boldsymbol{r}_i$ is the position of a point in link "i" with respect to inertial frame (the inertial coordinate frame being labeled as "0" and the base coordinate frame being labeled as "h"), then the velocity of the point in a segment can be expressed as in Eq. (7)

$${}^{0}\boldsymbol{v}_i = \frac{d}{dt}({}^{0}\boldsymbol{r}_i) \tag{7}$$

which can be re-written as Eq. (8)

$${}^{0}\boldsymbol{v}_i = \frac{d}{dt}({}^{0}\mathbf{A}_h\, {}^{h}\mathbf{A}_i\, {}^{i}\mathbf{r}_i) \tag{8}$$

where ${}^{h}\mathbf{A}_i$ is the homogenous transformation matrix describing the position and orientation of the ith link with respect to the reference base frames, whose elements are function of θ_i and ${}^{i}\boldsymbol{r}_i$ is the position of the point on the ith link with respect to the frame of reference distal to the link. ${}^{0}\mathbf{A}_h$ is the homogenous transformation matrix describing the translation of the hip joint frame with respect to the inertial frame given by

$${}^{0}\mathbf{A}_h = \begin{bmatrix} 1 & 0 & 0 & h_x \\ 0 & 1 & 0 & h_y \\ 0 & 0 & 1 & 0 \\ 0 & 0 & 0 & 1 \end{bmatrix} \tag{9}$$

where h_x and h_y are the X and Y position coordinates of the hip joint, with respect to the inertial frame. The homogenous transformation matrix of any ith segment will depend on the joint parameters of all the segments between itself and the reference base frame. Using the product rule of derivative, Eq. (8) can be expanded as

$${}^{0}\boldsymbol{v}_i = {}^{0}\dot{\mathbf{A}}_h\, {}^{h}\mathbf{A}_i\, {}^{i}\boldsymbol{r}_i + {}^{0}\mathbf{A}_h \sum_{j=1}^{i} \frac{\partial\, {}^{h}\mathbf{A}_i}{\partial \theta_j}\dot{\theta}_j\, {}^{i}\boldsymbol{r}_i \tag{10}$$

where ${}^{i}\dot{\boldsymbol{r}}_i = 0$ and $\frac{d}{dt}({}^{0}\mathbf{A}_h) = {}^{0}\dot{\mathbf{A}}_h$, θ_j is joint parameter for $j \in (1, 2, \ldots., i)$.

In the current study, as the lower limb is considered to have only revolute joints, the time derivative of the arm matrix can be expressed as

$$\begin{aligned} \frac{\partial\, {}^{i-1}\mathbf{A}_i}{\partial \theta_i} &= \begin{bmatrix} -\sin\theta_i & -\cos\alpha_i \sin\theta_i & \sin\alpha_i \sin\theta_i & -a_i \sin\theta_i \\ \cos\theta_i & -\cos\alpha_i \cos\theta_i & \sin\alpha_i \cos\theta_i & a_i \cos\theta_i \\ 0 & 0 & 0 & 0 \\ 0 & 0 & 0 & 0 \end{bmatrix} \\ &= \begin{bmatrix} 0 & -1 & 0 & 0 \\ 1 & 0 & 0 & 0 \\ 0 & 0 & 0 & 0 \\ 0 & 0 & 0 & 0 \end{bmatrix} \begin{bmatrix} \cos\theta_i & -\cos\alpha_i \sin\theta_i & \sin\alpha_i \sin\theta_i & a_i \cos\theta_i \\ \sin\theta_i & \cos\alpha_i \cos\theta_i & -\sin\alpha_i \cos\theta_i & a_i \sin\theta_i \\ 0 & \sin\alpha_i & \cos\alpha_i & d_i \\ 0 & 0 & 0 & 1 \end{bmatrix} \\ &= \mathbf{Q}_i\, {}^{i-1}\mathbf{A}_i \end{aligned} \tag{11}$$

where

$$\mathbf{Q}_i = \begin{bmatrix} 0 & -1 & 0 & 0 \\ 1 & 0 & 0 & 0 \\ 0 & 0 & 0 & 0 \\ 0 & 0 & 0 & 0 \end{bmatrix} \text{ for rotary joint [12]} \tag{12}$$

Kinetic Energy of the Lower Limb. The next step after finding the joint velocity of each segment is to calculate the kinetic energy of each segment. The kinetic energy dK_i of a point in link "i" with a differential mass dm can be expressed as

$$dK_i = \frac{1}{2}\,(\dot{x}_i^2 + \dot{y}_i^2 + \dot{z}_i^2)dm \tag{13}$$

$$dK_i = \frac{1}{2}\,Tr(\boldsymbol{v}_i \boldsymbol{v}_i^T)dm \tag{14}$$

where Eq. (14) can be expressed in the form of trace of a matrix by using the velocity vector of the ith link.

Substituting $\boldsymbol{v}_i$ from Eq. (8) in Eq. (14), the total kinetic energy of the complete lower-limb system is derived by summing energies of all segments, which can be expressed as

$$K = \sum_{i=1}^{n} \frac{1}{2} Tr({}^{0}\dot{\mathbf{A}}_h \, {}^{h}\mathbf{A}_i \, \mathbf{J}_i \, {}^{h}\mathbf{A}_i{}^{T} {}^{0}\dot{\mathbf{A}}_h^{T}) + \sum_{i=1}^{n} \sum_{a=1}^{i} Tr({}^{0}\dot{\mathbf{A}}_h \, {}^{h}\mathbf{A}_i \, \mathbf{J}_i \, \mathbf{U}_{ia}^{T} \, {}^{0}\mathbf{A}_h^{T}) \dot{\theta}_a + \frac{1}{2} \sum_{i=1}^{n} \sum_{a=1}^{i} \sum_{b=1}^{i} Tr({}^{0}\mathbf{A}_h \mathbf{U}_{ia} \, \mathbf{J}_i \mathbf{U}_{ib}^{T} \, {}^{0}\mathbf{A}_h^{T}) \dot{\theta}_a \dot{\theta}_b \tag{15}$$

where $\mathbf{J}_i = \int ({}^{i}\boldsymbol{r}_i)({}^{i}\boldsymbol{r}_i^{T}) dm$ is the inertia matrix of link "i" and n is the total number of links, $\mathbf{U}_{ij} = \dfrac{\partial \, {}^{h}\mathbf{A}_i}{\partial \theta_j}$, is a matrix which defines the rate of change of ${}^{i}\boldsymbol{r}_i$ as θ_j changes relative to the base coordinate frame [11,21]. In other words, $\boldsymbol{U}_{ij}$ is the effect of motion of joint "$\boldsymbol{J}$" on link or segment "$\boldsymbol{i}$". Similarly, $\mathbf{U}_{ijk} = \dfrac{\partial \mathbf{U}_{ij}}{\partial \theta_k}$ will also be another matrix describing inter-link interactions.

Potential Energy of the Lower Limb. The total potential energy of the lower limb is derived by summing the individual potential energies of each segment

$$P = \sum_{i=1}^{n} -m_i \boldsymbol{g} ({}^{0}\mathbf{A}_h \, {}^{h}\mathbf{A}_i \, {}^{i}\boldsymbol{r}_i) \tag{16}$$

where $\boldsymbol{g} = (0 \; 0 \; -\mathrm{g} \; 0)^{\mathrm{T}}$ is the gravity row vector with respect to inertial coordinate system and "g" is the acceleration due to gravity. The inertial frame of reference is assumed to have its Z-axis pointing upwards (as in Fig. 2(*a*)).

From Eqs. (16) and (17), the Lagrangian function, $L = K - P$ is given by

$$L = \sum_{i=1}^{n} \frac{1}{2} Tr({}^{0}\dot{\mathbf{A}}_h \, {}^{h}\mathbf{A}_i \, \mathbf{J}_i \, {}^{h}\mathbf{A}_i{}^{T} {}^{0}\dot{\mathbf{A}}_h^{T}) + \sum_{i=1}^{n} \sum_{a=1}^{i} Tr({}^{0}\dot{\mathbf{A}}_h \, {}^{h}\mathbf{A}_i \, \mathbf{J}_i \, \mathbf{U}_{ia}^{T} \, {}^{0}\mathbf{A}_h^{T}) \dot{\theta}_a + \frac{1}{2} \sum_{i=1}^{n} \sum_{a=1}^{i} \sum_{b=1}^{i} Tr({}^{0}\mathbf{A}_h \mathbf{U}_{ia} \, \mathbf{J}_i \mathbf{U}_{ib}^{T} \, {}^{0}\mathbf{A}_h^{T}) \dot{\theta}_a \dot{\theta}_b - \sum_{i=1}^{n} -m_i \boldsymbol{g} ({}^{0}\mathbf{A}_h \, {}^{h}\mathbf{A}_i \, {}^{i}\boldsymbol{r}_i) \tag{17}$$

After calculating the $\dfrac{\partial L}{\partial \dot{\theta}_i}$, $\dfrac{\partial L}{\partial \theta_i}$ terms, the final joint torque "τ_i" due to the motion of lower limb, without taking into consideration any external forces is given as

$$\tau_i = \sum_{j=i}^{n} Tr({}^{0}\dot{\mathbf{A}}_h \, {}^{h}\mathbf{A}_j \, \mathbf{J}_j \mathbf{U}_{ji}^{T} \, {}^{0}\mathbf{A}_h^{T}) + 2 \sum_{j=i}^{n} \sum_{r=1}^{j} Tr({}^{0}\dot{\mathbf{A}}_h \mathbf{U}_{jr} \, \mathbf{J}_j \mathbf{U}_{ji}^{T} \, {}^{0}\mathbf{A}_h^{T}) \dot{\theta}_r + \sum_{j=i}^{n} \sum_{r=1}^{j} \sum_{s=1}^{j} Tr(\mathbf{U}_{jrs} \mathbf{J}_j \mathbf{U}_{ji}^{T}) \dot{\theta}_r \dot{\theta}_s + \sum_{j=i}^{n} \sum_{r=1}^{j} Tr(\mathbf{U}_{jr} \, \mathbf{J}_j \mathbf{U}_{ji}^{T}) \ddot{\theta}_r + \sum_{j=1}^{n} m_j \boldsymbol{g} ({}^{0}\mathbf{A}_h \, {}^{h}\mathbf{A}_j \, {}^{j}\boldsymbol{r}_j) \tag{18}$$

Torque at Joints Due to Ground Reaction Force. During the swing phase, the joint torques are calculated from the kinematic and structural parameters of the leg alone. However, in the case of the stance phase of gait, the body experiences an additional external force when it comes in contact with the ground. This force is called GRF. The direction of GRF acting on the body during different instances of the stance phase is represented by Fig. 2(*a*). The magnitude of GRF during the same period is shown in Fig. 2(*b*). The GRF in the figure is plotted from dataset-3 [27] used in this study for validation of the proposed gait model. The magnitude and direction of the GRF vector are plotted to represent GRF during the stance phase.

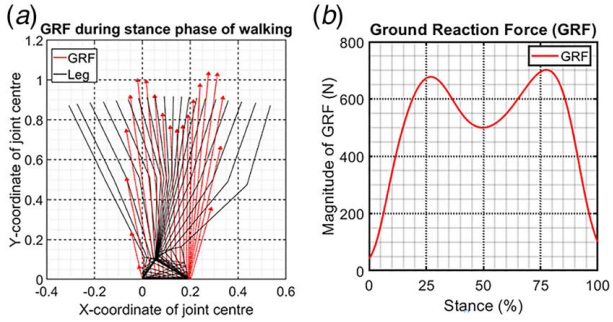

Fig. 2 (*a*) GRF during the stance phase and (*b*) the pattern of GRF during the stance phase

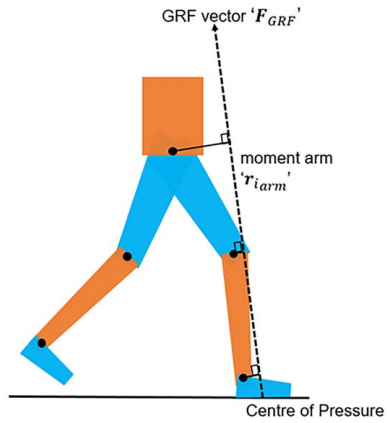

Fig. 3 Representation of GRF vector along with COP and moment arm

A force plate is commonly used in gait analysis to measure the GRF. The relative position of the GRF vector with respect to the joint axis is considered to calculate the resultant joint moment [22,28,29]. The measured ground reaction force vector is projected from the Cartesian space to the joint space using the distance of the projected GRF vector from the respective joint center ($\boldsymbol{r}_i arm$), as shown in Fig. 3. The total force applied by the foot on the ground is distributed throughout different points of the surface of the foot. However, for representation of the GRF as a vector, it is assumed to act at a point called COP.

To include the torques generated at the joints due to the ground reaction force, Eq. (18) can be written as

$$\boldsymbol{\tau}_{total-i} = \tau_i \; + \; (\boldsymbol{r}_i arm \; \times \; \boldsymbol{F}_{GRF}) \tag{19}$$

Hence, Eq. (19) can be written compactly in matrix form as

$$\boldsymbol{\tau} = \boldsymbol{D}(\boldsymbol{\theta})\ddot{\boldsymbol{\theta}} + \boldsymbol{h}(\boldsymbol{\theta}, \dot{\boldsymbol{\theta}}) + \boldsymbol{c}(\boldsymbol{\theta}) + \; \boldsymbol{F}_{\boldsymbol{ha}}(\boldsymbol{\theta}_{\boldsymbol{h}}, \; \dot{\boldsymbol{\theta}}_{\boldsymbol{h}})\dot{\boldsymbol{\theta}} + \boldsymbol{F}_{\boldsymbol{hb}}(\boldsymbol{\theta}_{\boldsymbol{h}}, \dot{\boldsymbol{\theta}}_{\boldsymbol{h}}, \ddot{\boldsymbol{\theta}}_{\boldsymbol{h}}) + \; \boldsymbol{\tau}_{\boldsymbol{GRF}} \tag{20}$$

where $\mathbf{D} = \begin{bmatrix} D_{11} & \cdots & D_{1n} \\ \vdots & \ddots & \vdots \\ D_{n1} & \cdots & D_{nn} \end{bmatrix}$, a $n \times n$ inertial acceleration-related symmetric matrix

$\boldsymbol{h}=[h_1, h_2, \ldots\ldots, h_n]^T$, a $n \times 1$ nonlinear Coriolis and centrifugal force vector

$\boldsymbol{c}=[c_1, c_2, \ldots\ldots, c_n]^T$, a $n \times 1$ gravity loading force vector

$\boldsymbol{F_{ha}} = [F_1, F_2, \ldots\ldots, F_n]^T$, a $n \times 1$ vector representing the inertia-like generalized forces induced by the hip motion on the lower limb

$\boldsymbol{F_{hb}} = \begin{bmatrix} F_{11} & \cdots & F_{1n} \\ \vdots & \ddots & \vdots \\ F_{n1} & \cdots & F_{nn} \end{bmatrix}$, a $n \times n$ matrix representing the Coriolis and centrifugal-like forces induced by the hip and the lower-limb motion on the lower limb.

$\boldsymbol{\tau}_{GRF} = [\boldsymbol{r}_1 arm \times \boldsymbol{F}_{GRF}, \ \boldsymbol{r}_2 arm \times \boldsymbol{F}_{GRF}, \ \ldots, \boldsymbol{r}_n arm \times \boldsymbol{F}_{GRF}]^T$, a $n \times 1$ vector representing the torque experienced at the lower-limb joints due to ground reaction force

$\boldsymbol{\theta}=[\theta_1, \theta_2, \ldots\ldots, \theta_n]^T$, a $n \times 1$ vector for generalized degrees-of-freedom.

The effect of moving base (${}^0\mathbf{A}_h$) can be observed in the final equation of the model. The derived model is used to simulate the gait dynamics, and is validated using three different datasets. The summary of the datasets used for validating the model is shown in Table 2.

The schematic diagram of the proposed model is shown in Fig. 4. The model was developed in MATLAB® environment.

Results and Discussion

In this section, the results of the study comparing the calculated joint torques obtained from the proposed model and the joint torques provided in the standard human gait datasets [12,27,30] are presented and discussed. Both the torque values for a particular joint are plotted in a single graph and compared visually. In addition to these plots, Bland–Altman plots are used to compare the two torques. Bland–Altman plot, or difference plot, is a graphical method to describe agreement between two quantitative measurements, with the use of limits of agreement [31]. In literature, this plot is found to be used to compare actual and estimated joint torques. The statistical limits are calculated using the mean and standard deviation of the differences between the two sets of torque values under comparison. The final graph is a scatter plot (XY) with the difference between the two torque values on the Y-axis, which is plotted against the mean of the two torques on the X-axis. The obtained results are discussed for each dataset.

Dataset-1: Hora et al. Dataset. The dataset provided in the work by Hora et al. [27] is the data of a walking individual in the sagittal plane. The numerical values of body mass, vertical GRF, joint marker coordinates, and COP coordinates are provided. The derived joint angles and joint moments are also provided in the dataset. In the work, the joint moments were calculated using link-segment equations, which act as the reference values against which our dynamic model is validated. The joint marker data at different frames are used to plot the stick diagram, as an illustration of the data in Fig. 5.

The joint torque values of the hip, knee, and ankle joints of both the calculated and dataset values are plotted with respect to stance percentage.

Table 2 Details of the dataset used for validation

S. no.	Name of the dataset	Gait type, phase, data source, format	Data type	Data given (units)
1	Hora et al. dataset [27]	Walking, stance phase, experimental, .csv format	Anthropometric data	• Body mass (68.5 kg) • Thigh length (mm), shank length (mm), and ankle height (mm)
			Temporal data	• Stance % (101 rows) • Frame time (0.00661 s)
			Kinematic data	• Hip–knee–ankle marker coordinates (m) • Joint angles (deg) • GRF data (N) • COP coordinates (m)
			Joint moments	Net hip, knee, and ankle moments (N-m) calculated using link-segment modeling
2	Winter. dataset [12]	Walking, swing–stance phase, experimental, .csv format	Anthropometric data	• Body mass (56.7 kg) • Thigh length (cm) • Shank length (cm) • Foot length (cm)
			Temporal data	• Frame (106 frames) • Frame rate (69.9 frames/s)
			Kinematic data	• Rib cage, hip, knee, ankle, metatarsal, toe marker coordinates (m) • Segment angles (deg) • Joint angles (deg) • GRF data (N) • CoP coordinates (m)
			Joint moments	Net hip, knee, and ankle moments (N-m)
3	Van den Bogert and De Koning [30]	Running, simulated, .zip format	Anthropometric data	• Segment mass (kg) • Moment of inertia (kg-m^2) • COM to proximal joint (% segment length) of thigh, shank, and foot segment
			Temporal data	• 6001 frames • Sampling interval of 0.1 ms • Heel strike at sample-3001
			Kinematic data	• Hip, knee, ankle, toe position coordinates (m) • Joint angles (deg) • GRF data (N) • COP coordinates (m)
			Joint moments	Net hip, knee, and ankle moments (N-m)

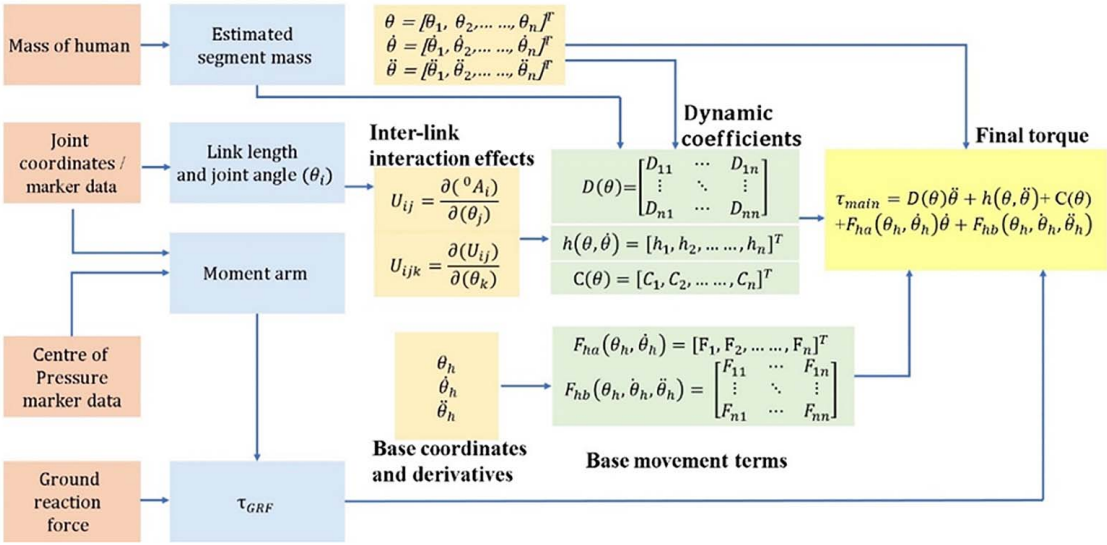

Fig. 4 Schematic diagram of formulation of the proposed gait model

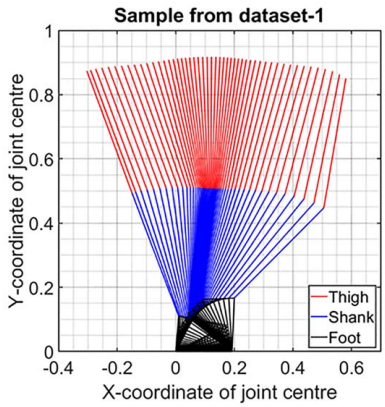

Fig. 5 Stick diagram of the stance phase from dataset-1

Through visual inspection of the torque plots in Fig. 6, the resemblance in trend between the calculated and reference values can be observed. As the authors have used the central-difference method for calculating the velocity and acceleration values, the first two and last two values of the data are zero, i.e., the values at stance percentages of 0, 1, 99, and 100 are zero and for the same instances the comparison is not performed. At the 21st stance value, a difference of 7.8 Nm is observed in the peak values of the torques for the hip joint. At this phase of stance, there is not much difference in the calculated and reference torque values for the knee and ankle joints. During the later phase of stance, i.e., at the 89th stance value, there is a difference of 10.9 Nm in hip torque values, while the difference in knee torques and ankle torques are 2.02 Nm and 0.34 Nm respectively at this stance.

To further evaluate the difference in calculated and reference joint torques, Bland–Altman plots were generated for each anatomical joint as shown in Fig. 7. The bias value (mean difference line) is −1.77, 0.005, and 0.001 for hip, knee, and ankle joints respectively. The bias is near zero, thereby suggesting that no systematic bias exists between the calculated and reference torques. The plots also indicate that the majority of data points are clustered between the limits of agreement, which is ±1.96% times the standard deviation of the differences. Though the Bland–Altman plot of knee and ankle torque appears to show an increasing trend as the reference torque increases, it can be observed from the plot that the difference in torque values is within the limit of 0.02 and 0.01 for knee and ankle respectively.

Dataset-2: Winter Dataset. This prominent gait data are sourced from the work by Winter [12]. The dataset includes 2D walking kinematic and force plate data. The kinematic data include marker data of the rib cage, hip, knee, fibula, ankle, heel, metatarsal, and toe while the force plate data include the GRF

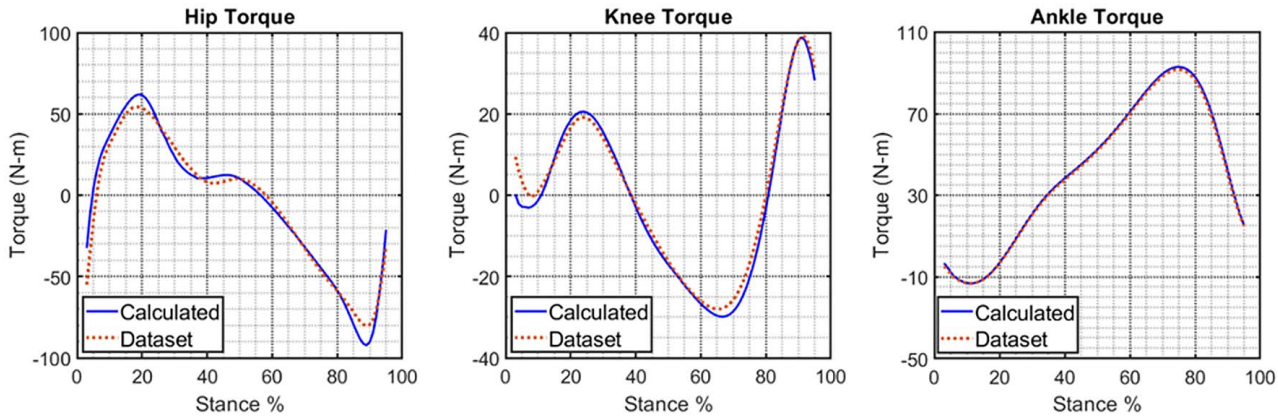

Fig. 6 Comparison of calculated and reference torques of dataset-1

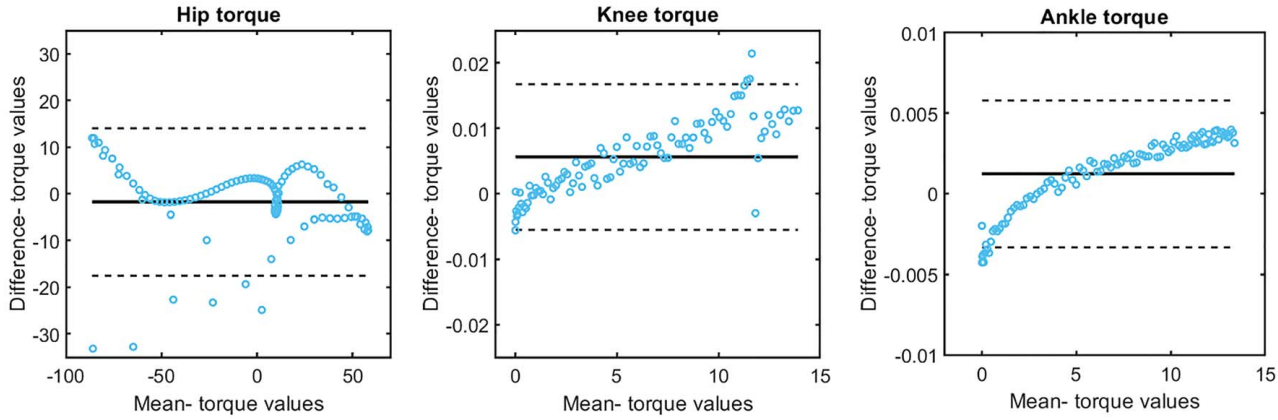

Fig. 7 Bland–Altman plot of calculated and reference torques of dataset-1

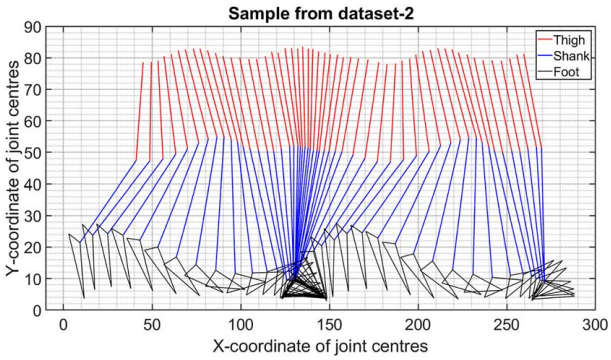

Fig. 8 Stick diagram of swing–stance phase from dataset-2

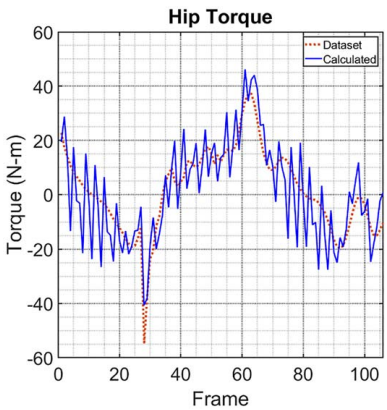

Fig. 9 Calculated hip torque without filtering

data along with COP data for every frame provided. The illustration of the walking subject is shown in Fig. 8.

Upon initial simulation of the proposed model using dataset-2, it was noticed that the calculated torque values contained undesired high-frequency noise for which an appropriate low-pass digital filter was used. For example, the calculated hip torque includes a lot of noise as shown in Fig. 9.

The selection of type of filter and its related parameters are not considered in the scope of this study. However, for the purpose of comparison, the noisy data pertaining to this dataset was smoothed using the "*smoothdata*" function of MATLAB®, which returns a moving average of the calculated data using a fixed window length that is determined heuristically. The joint torque after performing the smooth function is compared, which is plotted as shown in Fig. 10.

The initial visual inspection in Fig. 11 indicates that the calculated and the reference torques match in terms of trend. The values provided in the dataset are "frame" wise, with 106 frames. Differences in joint torque values can be observed in the initial few frames, which can be attributed to the calculation of velocity or acceleration terms using the central difference method. Considering the difference at peaks, a difference of 8.75 Nm in hip torque, and 7.14 Nm in knee torque is observed at the 28th frame. A difference of 3.5 Nm is observed in knee torque at the 37th frame. The Bland–Altman plots for examining the model performance for this dataset are shown in Fig. 11.

The bias value (central horizontal line) is 1.01, 0.06, and 0.001 for hip, knee, and ankle torques respectively. The data points are spread around the centerline and mostly lie between the limits of agreement. Though data points are sloping upward from left to right in the case of knee and ankle torques, the difference is only around 0.01 and 0.005 for knee and ankle torques respectively.

Dataset-3: Van den Bogert and De Koning Dataset. The dataset contains files generated by the direct dynamic simulation of running, sourced from the work of Van den Bogert and De Koning [30]. The inertial properties of the 2D musculoskeletal model used in the simulation along with position data of hip, knee, ankle, and toe are given in the dataset. The illustration of lower limb movement pertaining to this dataset is shown in Fig. 12. The GRF data along with the *x*-coordinate of COP are also given. Additionally, the joint moments calculated using link-segment modeling are given in the dataset, which is used as the reference values for comparing joint torques.

The joint torques of the calculated and reference torque value for this dataset are plotted in Fig. 13.

The joint torques are plotted for every "frame," starting from the 3001st frame when the heel strike occurs. The comparison plots show an overall correspondence between the torque values obtained through the proposed model and the reference dataset. The graph indicates that the calculated hip torque and knee torque have anomalies near the 3147th frame. In the paper by Van den Bogert and De Koning [30], where the current dataset was used, the type of filter and the parameters to avoid these anomalies were discussed. The cutoff frequencies ranged from 3.0 Hz to 94.3 Hz, varying for force and torque measurements, and further differing across the hip, knee, and ankle joints. As the authors have presented the joint torque results for the cutoff frequency of 15.1 Hz, a second-order Butterworth filter with the same cutoff frequency was used in the present study. The comparison plots after the application of the digital filter are shown in Fig. 14.

The burst in the hip torque of Fig. 13 is actually an artificial noise introduced in the simulation data by Van den Bogert and De Koning

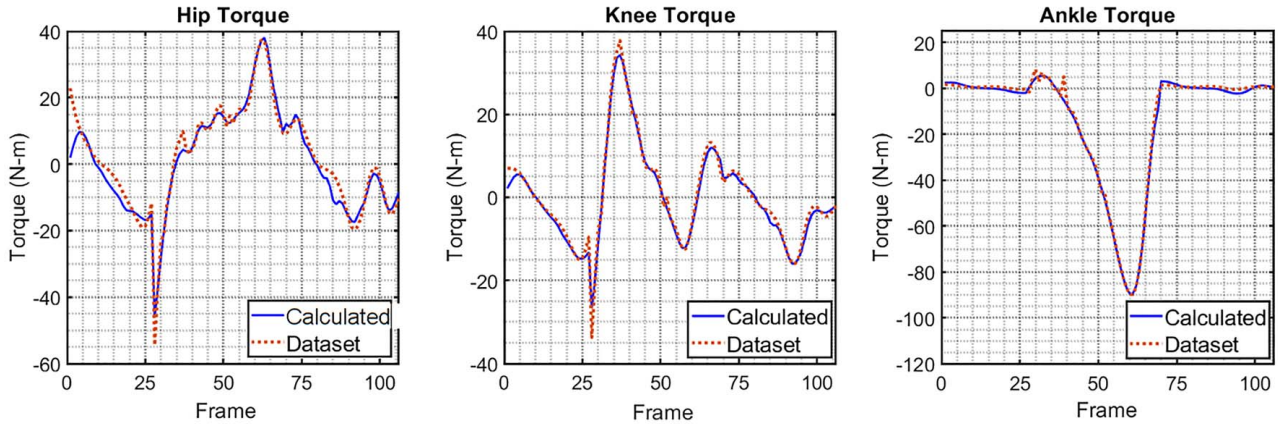

Fig. 10 Comparison of calculated and reference torques of dataset-2

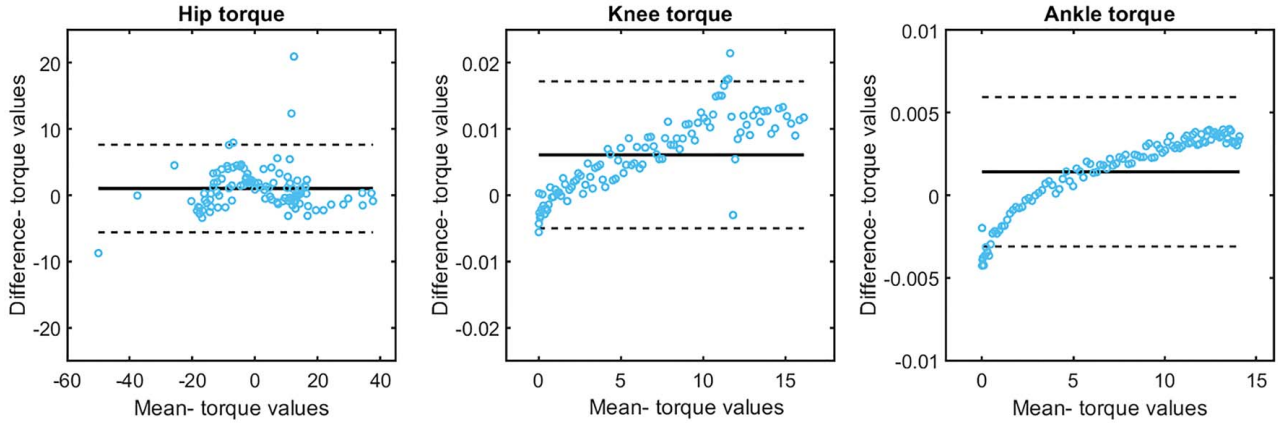

Fig. 11 Bland–Altman plot of calculated and reference torques of dataset-2

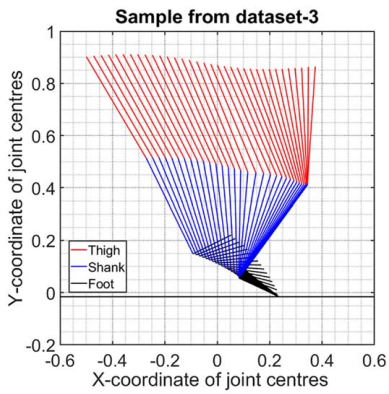

Fig. 12 Stick diagram of stance phase from dataset-3

[30]. Similarly, as illustrated in Fig. 14, a similar burst is evident in the hip torque data presented by Van den Bogert and De Koning [30] at a cutoff frequency of 15.1 Hz. In the current research work, the authors did not include optimal filtering as a component of the study; rather, solely utilized the dataset for validating the model.

The calculated torque values after filtering are used for comparison in the Bland–Altman plot for this dataset, as shown in Fig. 15.

It can be observed that the data points are evenly distributed around the bias line and mostly within the limits of agreement. This is indicative of a strong overall agreement of the proposed model for this dataset. The bias has near-zero values for hip, knee, and ankle torques, which also suggests the minimal bias between the torque values.

In addition to the Bland–Altman plots, the MAE and mean error (ME) were also calculated to assess the accuracy of the proposed model. The values of the mean absolute error and the mean error are tabulated in Tables 3 and 4 respectively.

From the above table, it can be noticed that the MAE in estimating hip joint torque is relatively higher in dataset-1 and dataset-2. Upon visual inspection, such as in Fig. 6 for dataset-1 [27] and Fig. 10 for dataset-2 [12], it can be observed that in some instances the estimated hip torque values do not match with reference values. This could be due to the difference in numerical estimation of joint velocity and acceleration values. It was observed through calculations that the MAE in case of hip torque of Hora et al. [27] reduced to around 3.00 N-m when the initial and final values were not compared.

The acceleration values of these datasets (dataset-1 and dataset-2) may be filtered initially, whose information is not provided along with the dataset. The selection of digital filter parameters also contributes to the final calculated values. Also, for these two datasets, the parameters like segment masses, segment lengths, and location of center of mass were estimated in this paper using a particular body-segment parameters estimation technique. This technique may differ from the actual one used in the original dataset papers. The values of these parameters vary with respect to the estimation models adopted. The effect of different body segments' parameter estimation models on the calculation of lower-limb joint torques

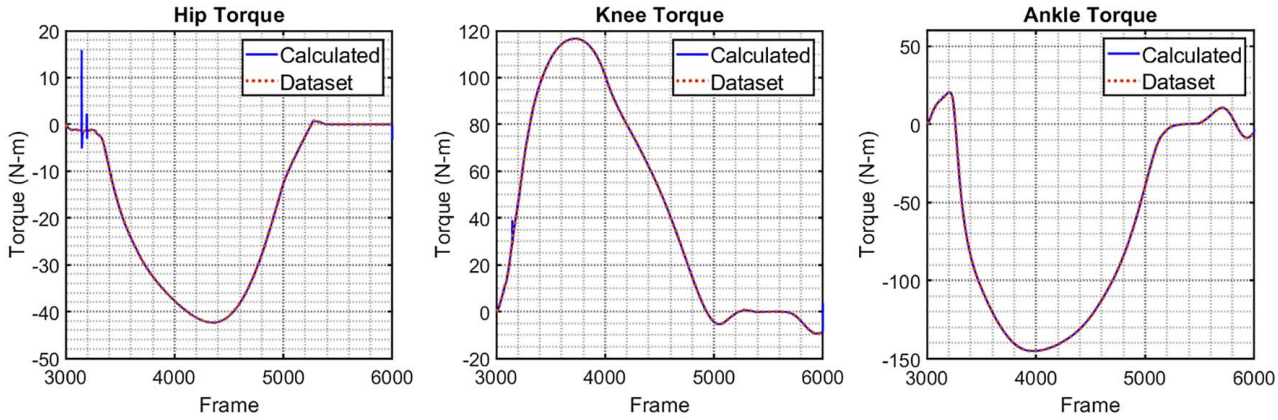

Fig. 13 Comparison of unfiltered-calculated and reference torques of dataset-3

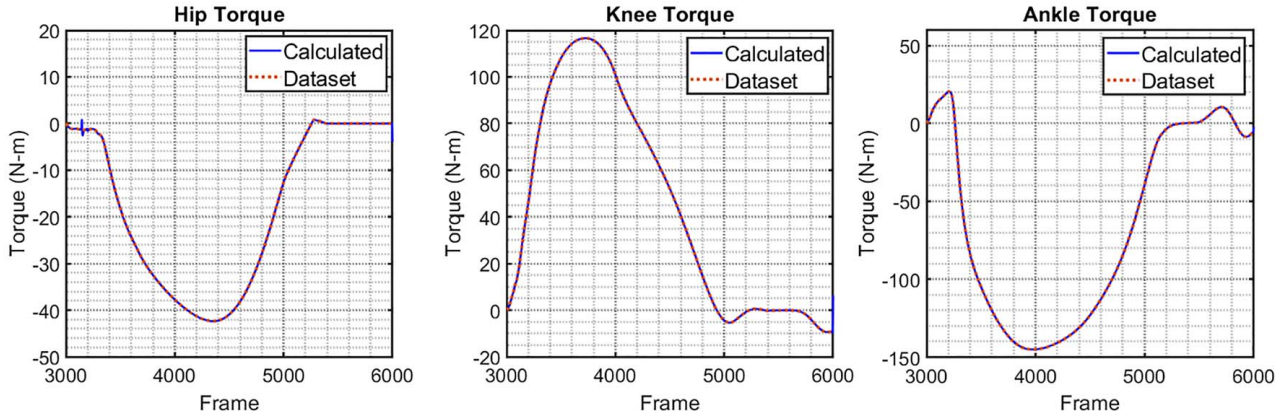

Fig. 14 Comparison of filtered-calculated and reference torques of dataset-3

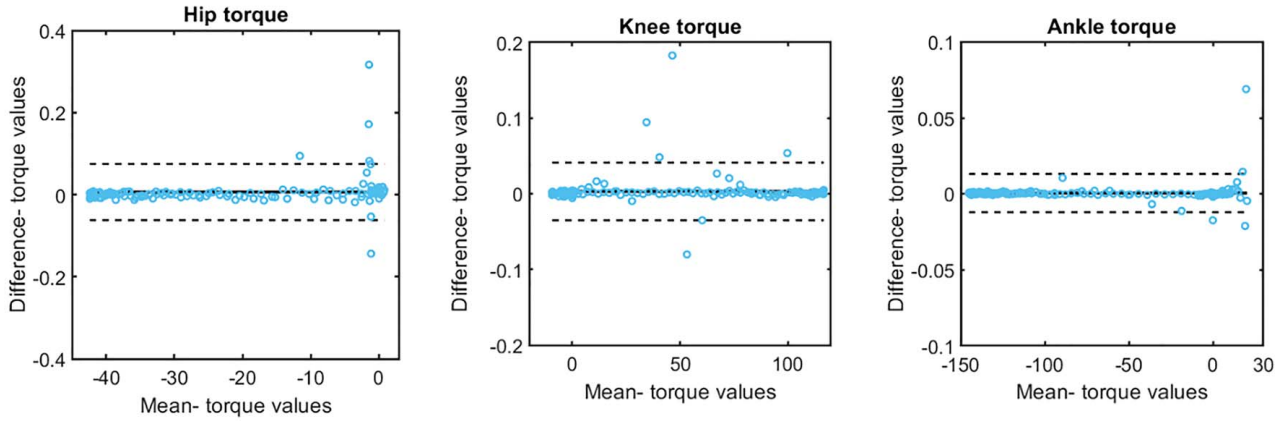

Fig. 15 Bland–Altman plot of calculated and reference torques of dataset-3

Table 3 MAE of joint torques (N-m)

Dataset no.	Hip joint	Knee joint	Ankle joint
1. Hora et al. [27]	4.17	1.58	0.86
2. Winter [12]	2.30	1.02	1.06
3. Van den Bogert and De Koning [30]	0.02	0.02	0.00

Table 4 ME of joint torques (N-m)

Dataset no.	Hip joint	Knee joint	Ankle joint
1. Hora et al. [27]	−0.87	1.09	−0.85
2. Winter [12]	1.01	0.55	0.53
3. Van den Bogert and De Koning [30]	0.00	−0.01	0.00

was previously reported by Rao et al. [32]. In the case of dataset-3, the segment mass value, center-of-mass location with respect to the proximal joint, and moment of inertia values were provided in the dataset itself. Therefore, the difference between calculated and reference torques in this case was minimal. Overall, the time-series plots, Bland–Altman plots, and error value calculation across the three datasets collectively indicate that the proposed dynamic formulation proves effective in estimating joint torques during human motion.

Conclusion

In this study, the Euler–Lagrange-based dynamic formulation for robotic manipulators was modified such that the reference base frame is non-inertial so that the formulation can be used for human gait analysis as well. Though the approach is developed for human gait in the sagittal plane, the same approach can be extended to the analysis of human gait in other anatomical planes too. The developed model was validated with three different datasets, which are diverse and cover a wide range of scenarios including the stance phase-swing phase of human walking, simulated-experimental data of gait, and running-walking activity of humans. In the three datasets reported in the paper, the joint torques are derived using the Newton–Euler or link-segment method, whereas the authors have used the modified Euler–Lagrange method to calculate the same. The near-zero bias between both approaches validates the proposed approach toward the estimation of joint torques in human gait. The developed model holds the potential not only toward understanding of human gait mechanics but also can contribute to broader biomechanical studies involving prosthetics or exoskeletons.

Acknowledgment

The authors would like to thank the Science and Engineering Research Board, Government of India for funding the project through grant CRG/2022/005578.

Conflict of Interest

The authors have no competing interest to declare. All co-authors have seen and agree with the contents of the manuscript and there is no financial interest to report. We certify that the submission is original work and is not under review at any other publication.

Data Availability Statement

In this study, the authors utilized open data, which is freely available and does not require copyright permission for use. The datasets of human gait that are used in this study are available in Refs. [12,27,30] or through online.[2]

The authors declare that all other data generated during and/or analyzed during the current study are available from the corresponding author on reasonable request.

References

[1] Marshall, E. A., 1983, "A Dynamical Model for the Stride in Human Walking," Math. Modell., **4**(5), pp. 391–415.

[2] Tutsoy, O., Erol Barkana, D., and Colak, S., 2017, "Learning to Balance an NAO Robot Using Reinforcement Learning With Symbolic Inverse Kinematic," Trans. Inst. Meas. Control, **39**(11), pp. 1735–1748.

[3] Zhang, L., Soselia, D., Wang, R., and Gutierrez-Farewik, E. M., 2022, "Lower-Limb Joint Torque Prediction Using LSTM Neural Networks and Transfer Learning," IEEE Trans. Neural Syst. Rehabil. Eng., **30**, pp. 600–609.

[4] Omer, A., Hashimoto, K., Lim, H. O., and Takanishi, A., 2014, "Study of Bipedal Robot Walking Motion in Low Gravity: Investigation and Analysis," Int. J. Adv. Rob. Syst., **11**(9), p. 139.

[5] Hong, H., Kim, S., Kim, C., Lee, S., and Park, S., 2013, "Spring-Like Gait Mechanics Observed During Walking in Both Young and Older Adults," J. Biomech., **46**(1), pp. 77–82.

[6] Gora, S., Gupta, S. S., and Dutta, A., 2023, "Energy-Based Footstep Planning of Biped on Uneven Deformable Terrain Using Nonlinear Inverted Pendulum," ASME J. Mech. Rob., **15**(5), p. 054502.

[7] Ren, L., Jones, R. K., and Howard, D., 2008, "Whole Body Inverse Dynamics Over a Complete Gait Cycle Based Only on Measured Kinematics," J. Biomech., **41**(12), pp. 2750–2759.

[8] Alkjaer, T., Simonsen, E. B., and Dyhre-Poulsen, P., 2001, "Comparison of Inverse Dynamics Calculated by Two- and Three-Dimensional Models During Walking," Gait Posture, **13**(2), pp. 73–77.

[9] Maillardet, F. J., 1977, "The Swing Phase of Locomotion," Eng. Med., **6**(3), pp. 101–106.

[10] Vimieiro, C., Andrada, E., Witte, H., and Pinotti, M., 2015, "A Computational Model for Dynamic Analysis of the Human Gait," Comput. Meth. Biomech. Biomed. Eng., **18**(7), pp. 799–804.

[11] Fu, K. S., Gonzalez, R. C., Lee, C. G., and Freeman, H., 1987, *Robotics: Control, Sensing, Vision, and Intelligence*, Vol. 1, McGraw-Hill, New York.

[12] Winter, D. A., 2009, *Biomechanics and Motor Control of Human Movement*, John Wiley & Sons, Hoboken, NJ.

[13] Al-Shuka, H. F., Corves, B. J., and Zhu, W. H., 2014, "Dynamic Modeling of Biped Robot Using Lagrangian and Recursive Newton-Euler Formulations," Int. J. Comput. Appl., **101**(3), pp. 1–8.

[14] Xiang, Y., Arora, J. S., Rahmatalla, S., and Abdel-Malek, K., 2009, "Optimization-Based Dynamic Human Walking Prediction: One Step Formulation," Int. J. Numer. Methods Eng., **79**(6), pp. 667–695.

[15] Tu, Y., Zhu, A., Song, J., Shen, H., Shen, Z., Zhang, X., and Cao, G., 2020, "An Adaptive Sliding Mode Variable Admittance Control Method for Lower Limb Rehabilitation Exoskeleton Robot," Appl. Sci., **10**(7), p. 2536.

[16] Velandia, C. C., Tibaduiza, D. A., and Vejar, M. A., 2017, "Proposal of Novel Model for a 2 DOF Exoskeleton for Lower-Limb Rehabilitation," Robotics, **6**(3), p. 20.

[17] Tutsoy, O., and Barkana, D. E., 2021, "Model Free Adaptive Control of the Under-Actuated Robot Manipulator With the Chaotic Dynamics," ISA Trans., **118**, pp. 106–115.

[18] Featherstone, R., 2014, *"Rigid Body Dynamics Algorithms"*, Springer, New York.

[19] Sentis, L., and Khatib, O., 2005, "Control of Free-Floating Humanoid Robots Through Task Prioritization," Proceedings of the 2005 IEEE International Conference on Robotics and Automation, Barcelona, Spain, April, IEEE, pp. 1718–1723.

[20] McGrath, M., Howard, D., and Baker, R., 2017, "A Lagrange-Based Generalised Formulation for the Equations of Motion of Simple Walking Models," J. Biomech., **55**, pp. 139–143.

[21] Wronka, C. M., and Dunnigan, M. W., 2011, "Derivation and Analysis of a Dynamic Model of a Robotic Manipulator on a Moving Base," Rob. Auton. Syst., **59**(10), pp. 758–769.

[22] Apkarian, J., Naumann, S., and Cairns, B., 1989, "A Three-Dimensional Kinematic and Dynamic Model of the Lower Limb," J. Biomech., **22**(2), pp. 143–155.

[23] Qi, Y., Soh, C. B., Gunawan, E., Low, K. S., and Maskooki, A., 2013, "A Novel Approach to Joint Flexion/Extension Angles Measurement Based on Wearable UWB Radios," IEEE J. Biomed. Health Inform., **18**(1), pp. 300–308.

[24] Drillis, R., Contini, R., and Bluestein, M., 1964, "Body Segment Parameters," Artif. Limbs, **8**(1), pp. 44–66.

[25] Vaughan, C. L., Davis, B. L., and O'connor, J. C., 1992, *Dynamics of Human Gait*, Human Kinetics Publishers, South Africa.

[26] Contini, R., 1972, "Body Segment Parameters, Part II," Artif. Limbs, **16**(1), pp. 1–19.

[27] Hora, M., Soumar, L., Pontzer, H., and Sládek, V., 2017, "Body Size and Lower Limb Posture During Walking in Humans," PLoS One, **12**(2), p. e0172112.

[28] Whittle, M. W., 2014, *Gait Analysis: An Introduction*, Butterworth-Heinemann Elsevier, Philadelphia, PA.

[29] Wells, R. P., 1981, "The Projection of the Ground Reaction Force as a Predictor of Internal Joint Moments," Bull. Prosthet. Res., **10**, pp. 15–19.

[30] Van den Bogert, A. J., and De Koning, J. J., 1996, "On Optimal Filtering for Inverse Dynamics Analysis," Proceedings of the IXth Biennial Conference of the Canadian Society for Biomechanics, Vancouver, Canada, Aug. 21–24, pp. 214–215.

[31] Giavarina, D., 2015, "Understanding Bland Altman Analysis," Biochem. Med., **25**(2), pp. 141–151.

[32] Rao, G., Amarantini, D., Berton, E., and Favier, D., 2006, "Influence of Body Segments' Parameters Estimation Models on Inverse Dynamics Solutions During Gait," J. Biomech., **39**(8), pp. 1531–1536.

[2] https://isbweb.org/data/ and https://onlinelibrary.wiley.com/doi/10.1002/9780470549148.app1.